

Optical properties of the fiber-optic temperature sensor based on the side-hole fiber filled with indium

Bok Hyeon Kim,^{1,4} Seung Ho Lee,² Dong Hoon Son,² Tae-Jung Ahn,³
So Eun Kim,¹ and Won-Taek Han^{2,5}

¹Advanced Photonics Research Institute, Gwangju Institute of Science and Technology (GIST),
Gwangju 500-712, South Korea

²Graduate Program of Photonics and Applied Physics, School of Information and Communications,
Gwangju Institute of Science and Technology (GIST), Gwangju 500-712, South Korea

³Department of Photonic Engineering, Chosun University, Gwangju 501-759, South Korea

⁴e-mail: bhkim@gist.ac.kr

⁵e-mail: wthan@gist.ac.kr

Received 28 September 2012; revised 26 December 2012; accepted 31 December 2012;
posted 4 January 2013 (Doc. ID 176601); published 30 January 2013

A highly sensitive temperature sensor was made by use of a side-hole glass fiber filled with indium metal, and its optical properties were investigated. The temperature sensitivity of the fiber-optic temperature sensor was $d\lambda/dT = -7.38$ nm/K. The temperature sensitivity was also examined in sensors made by different lengths of the side-hole fiber and the indium-filled fiber region. The temperature sensitivity could be varied in the range of -1.83 to -7.38 nm/K by changing the relative length between the side-hole fiber and the indium-filled fiber region. © 2013 Optical Society of America

OCIS codes: 060.2370, 060.2400, 060.2290.

1. Introduction

Fiber-optic sensors based on glass optical fibers have been extensively studied because glass fibers have attractive features, such as high sensitivity, time and spectral multiplicity, large chemical stability, and device compactness. Various types of fiber-optic temperature sensors have been exploited; fiber Bragg gratings and long-period fiber gratings have especially attracted great interest in temperature-sensing applications [1–3]. However, the fiber sensors have several drawbacks, such as a high sensitivity to bending and polarization and a low sensitivity to temperature. On the other hand, fiber-optic sensors based on birefringent fibers have shown several advantages: high temperature sensitivity, robust characteristics

on bending and polarization, and large tunability on a spectral bandwidth [2,4].

Up to now, various optical fibers have been incorporated with metals, and their properties, such as electro-optic effect [5–7], current-induced birefringence change [8], metallic mode confinement [9], and surface plasmon resonance [10] were investigated. Recently, we have demonstrated a new type of birefringent fiber that has an elliptical core and side holes filled with metals [11,12]. The temperature sensitivity of the fiber was significantly enhanced by filling the holes with metals having large thermal expansion properties. In particular, the side-hole fiber filled with indium metal exhibited very large temperature sensitivities on wavelength shift ($d\lambda/dT = -6.3$ nm/K) and birefringence change ($dB/dT = -3.32 \times 10^{-6}$ /K), and they were 10 and 60 times larger than those of the fiber without the metal, respectively [11]. The effect of filler metals (Bi, 80Au–20Sn alloy, Sn, and In) on the temperature

sensitivity of the side-hole fiber was also investigated using Sagnac loop interferometry [12]. The optical properties of the fiber were found to be significantly affected by the types of filler metals inside the fibers. The magnitude of the fiber birefringence and the temperature sensitivity increased with the increase of the thermal expansion coefficients of the metals.

More recently, we have proposed a fiber-optic temperature sensor with high temperature sensitivity as well as a simple end-face optical configuration [13]. The sensor was composed of a side-hole fiber connected to a fiber-pigtailed polarization beam splitter (PBS), and the end face of the side-hole fiber was mirror coated with aluminum. The end region of the side-hole fiber was filled with indium and was used as a sensing element of the device. The proposed fiber-optic sensor was found to have the very large temperature sensitivity of $d\lambda/dT = -7.5$ nm/K at 1400 nm, which is much larger than that of the most sensitive sensors reported so far, $d\lambda/dT = -1$ to -2 nm/K [2,4]. In this study, we made fiber-optic temperature sensors with different lengths of the side-hole fiber and the indium-filled fiber region, and the optical properties of the sensors were experimentally investigated and compared with the theoretical expectation. It was found that the optical properties of the sensors were strongly affected by the relative length between the side-hole fiber and the indium-filled fiber region.

2. Experiments

Using the conventional modified chemical vapor deposition process, an optical fiber preform with a germanium-doped core was fabricated, and the two holes beside the core of the preform were made by a mechanical drilling process. The preform was drawn into the side-hole fiber with an elliptical core, and the hole was slightly collapsed to introduce the fiber birefringence. During the fiber-drawing process, the drawing temperature and the drawing speed were properly controlled to make the fiber with cladding and hole diameters of 125 and ~ 20 μm , respectively. Molten indium at 180°C was infiltrated into the side-holes of the fiber by the aid of nitrogen gas at a pressure of ~ 27 bars [7,11,14] to introduce the large thermal-expansion property mismatch from silica glass with $\alpha = 5.5 \times 10^{-7}/\text{K}$ used as the fiber cladding material. It is noted that the thermal

expansion coefficient and the melting temperature of indium are $\alpha = 32.1 \times 10^{-6}/\text{K}$ and 156°C, respectively [15]. Figure 1 shows cross-sectional microphoto images of the fiber obtained before and after the metal infiltration process and a scanning electron microscopy (SEM) image of the side-hole region filled with indium. As shown in the figure, an elliptical core was found at the center of the fiber with the two holes beside the fiber core, and the metal indium was well incorporated inside the holes. Glittering spots observed in the indium-filled side-hole region of the photo image resulted from the reflection of light at the metal surface.

The schematic structure of the fiber-optic temperature sensor is presented in Fig. 2. The optical configuration of the sensor was similar to that of the polarimetric interferometer [7], and the sensing part of the device was made by the side-hole fiber filled with indium. Up to now, most fiber-optic temperature sensors made by birefringent fibers have been studied with the Sagnac fiber-loop interferometer [2,4,11,12]. Compared with the sensor in the fiber-loop configuration, the straight end-face-type sensor exhibits the advantages of simplicity and compactness in the device structure.

In a fiber-optic sensor (sensor A), the total length of the side-hole fiber was 100 cm (L) and the length of the indium-filled fiber region was 20 cm (L_m). The end of the side-hole fiber was mirror coated with aluminum to increase the optical reflection. Broadband light was launched into the input port of the fiber-pigtailed PBS and was coupled to the side-hole optical fiber after passing through the transmitted fiber port of the PBS. Then the light was backreflected at the aluminum-coated fiber end, and the output spectrum was measured using an optical spectrum analyzer (Ando, AQ 6317B). A fiber polarization controller was used to optimize the interference fringe spectrum. The 50 cm long part (L_p) of the side-hole fiber from the end face, including the 20 cm long fiber region filled with indium, was heated at a temperature of 25°C to 83°C using an electrically controlled thermal chamber. Thus, the heated length of the side-hole fiber without indium inside the thermal chamber was 30 cm ($L_n = L_p - L_m$). As a reference, the characteristics of the fiber-optic sensor made by the side-hole fiber without indium were examined with the same experimental conditions, such as the

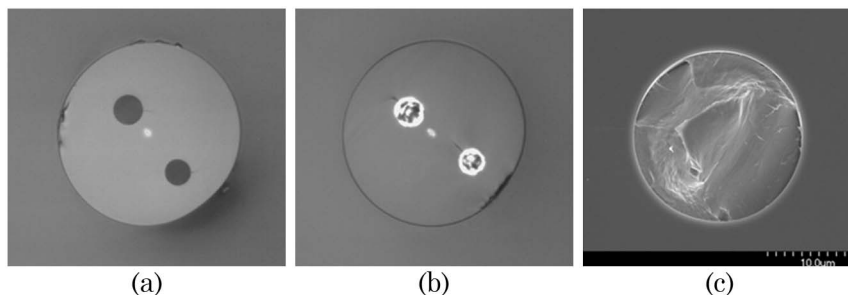


Fig. 1. Microphoto images of the side-hole fiber (a) before and (b) after the metal infiltration process, and (c) SEM image of the indium-filled side-hole region near the elliptical core.

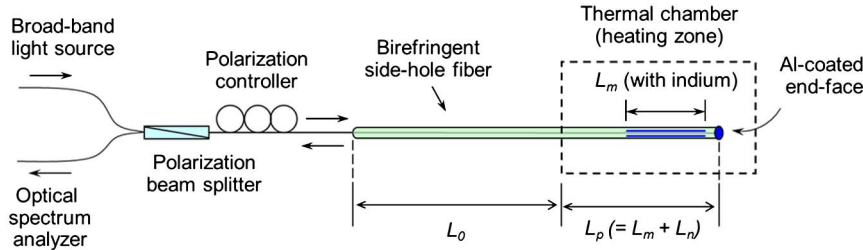


Fig. 2. (Color online) Schematic structure of the end-face-type fiber-optic temperature sensor made with the side-hole fiber with the indium-filled fiber region near the fiber end face.

total length of the sensor fiber, the heated length of the fiber, and the temperature range.

Fiber-optic temperature sensors were also made by using different lengths of the side-hole fiber and indium-filled fiber region, and their optical properties were investigated. In sensor B, the 50 cm long side-hole fiber with the 2 cm long indium-filled fiber region was used. In the other cases, 25 cm long side-hole fibers with 2 and 5 cm long fiber regions filled with indium were used for fiber sensors C and D, respectively. Temperature sensitivities of the sensors with the different features were examined with the same experimental procedure conducted for sensor A. The sensor fibers were connected to the transmitting fiber port of the PBS, and the 50 cm long fiber regions from the end face including the indium-filled fiber regions were heated using the thermal chamber; then the output spectra were investigated during the elevation of the temperature up to 85°C.

3. Operation Principle

The transmission properties of the Sagnac loop interferometers (SLIs) made by the birefringent side-hole fibers filled with metals have been described in previous studies [11,12]. On the basis of similar considerations, the operation characteristics of the fiber-optic temperature sensor made by the indium-filled side-hole fiber were exploited in this study. The transmission of the fiber-optic sensor is given by the periodic form $T = \sin^2(\varphi/2)$, where φ is the birefringence-induced phase difference between the principal polarization modes of the fiber core. Because light propagates the round trip of the sensor fiber, the phase difference becomes twofold from that of the conventional SLI and is expressed as $\varphi = 4\pi BL/\lambda$, where B is the fiber birefringence, λ is the wavelength, and L is the length of the side-hole fiber. The fringe spacing, or the spectral separation of the interference fringe in the transmission, is given by $S = \lambda^2/(2BL)$, thus $\varphi = 2\pi\lambda/S$ [16].

The sum of the phase differences arising at each of the segmented fiber regions gives the total phase difference, φ_t , as follows:

$$\begin{aligned} \varphi_t(T) &= \varphi_m(T) + \varphi_n(T) + \varphi_0 = \frac{4\pi BL}{\lambda} = \frac{2\pi\lambda}{S} \\ &= \frac{4\pi(B_m L_m + B_n L_n + B_0 L_0)}{\lambda}, \end{aligned} \quad (1)$$

thus

$$\frac{\lambda}{S} = \frac{2(B_m L_m + B_n L_n + B_0 L_0)}{\lambda}, \quad (2)$$

where $B_m L_m$ and $B_n L_n$ are the birefringence-length products for the fiber regions with and without indium inside the heating chamber, respectively, and $B_0 L_0$ is the product for the fiber region without indium outside the chamber. In the equation, B indicates the effective fiber birefringence that manifests the overall property of the side-hole fiber.

From Eq. (1), the fringe spacing is expressed as a function of the birefringence-length products of the segmented regions,

$$S = \frac{\lambda^2}{2BL} = \frac{\lambda^2}{2(B_m L_m + B_n L_n + B_0 L_0)}, \quad (3)$$

where $L = L_m + L_n + L_0$. Therefore, the birefringence, B_m , in the fiber region with indium at the varied temperature is derived as

$$B_m = \frac{L}{L_m} B - \frac{L_n}{L_m} B_n - \frac{L_0}{L_m} B_0. \quad (4)$$

As a reference, the birefringence, B_n , in the fiber region without indium can be obtained by use of the reference side-hole fiber without indium,

$$B_n = \frac{L}{L_p} B - \frac{L_0}{L_p} B_0, \quad (5)$$

where $L_p = L_m + L_n$. The variation of the fiber length owing to the thermal expansion property of the fiber is ignored in the equations. The fiber birefringence, B_s , solely induced by indium can be estimated by subtracting B_n of the reference fiber from B_m of the fiber with indium:

$$B_s = B_m - B_n = \frac{L}{L_m} B - \left(\frac{L_n}{L_m} + 1\right) B_n - \frac{L_0}{L_m} B_0. \quad (6)$$

From Eq. (2), the temperature derivation of the phase difference gives

$$\frac{\delta}{\delta T} \left(\frac{\lambda}{S} \right) = \frac{\delta}{\delta T} \left[\frac{2(B_m L_m + B_n L_n + B_0 L_0)}{\lambda} \right]. \quad (7)$$

During the variation of the temperature, the wavelength shift with constant fringe spacing (in the left side) can be obtained from the temperature derivation of the birefringence-length product terms at a fixed wavelength (in the right side) [17]; thus the equation becomes

$$\frac{1}{S} \frac{d\lambda}{dT} = \frac{2}{\lambda} \frac{\delta}{\delta T} (B_m L_m + B_n L_n + B_0 L_0), \quad (8)$$

$$\begin{aligned} \frac{d\lambda}{dT} &= \frac{2S}{\lambda} \frac{\delta}{\delta T} (B_m L_m + B_n L_n + B_0 L_0) \\ &= \frac{2S}{\lambda} \left[B_m L_m \left(\frac{1}{B_m} \frac{\delta B_m}{\delta T} + \frac{1}{L_m} \frac{\delta L_m}{\delta T} \right) \right. \\ &\quad \left. + B_n L_n \left(\frac{1}{B_n} \frac{\delta B_n}{\delta T} + \frac{1}{L_n} \frac{\delta L_n}{\delta T} \right) \right]. \end{aligned} \quad (9)$$

In the side-hole fibers with and without indium, the thermal expansion coefficients $\alpha = 1/L_m \delta L_m / \delta T \approx 1/L_n \delta L_n / \delta T = 5.5 \times 10^{-7} \text{ K}^{-1}$ are three to four orders smaller than those values of $1/B_m \delta B_m / \delta T \approx -3.30 \times 10^{-6} / 2.00 \times 10^{-4} \text{ K}^{-1} \approx -1.65 \times 10^{-3} \text{ K}^{-1}$ and $1/B_n \delta B_n / \delta T \approx -2.70 \times 10^{-8} / 1.06 \times 10^{-4} \text{ K}^{-1} \approx -2.55 \times 10^{-4} \text{ K}^{-1}$ (see the optical characteristics given in Table 1). Thus, the equation becomes

$$\frac{d\lambda}{dT} \approx \frac{2S}{\lambda} \left[\frac{\delta B_m}{\delta T} L_m + \frac{\delta B_n}{\delta T} L_n \right]. \quad (10)$$

Because the magnitude of $\delta B_n / \delta T = -2.70 \times 10^{-8} \text{ K}^{-1}$ in the fiber without indium is much smaller than that of the fiber with indium ($\delta B_m / \delta T = -3.30 \times 10^{-6} \text{ K}^{-1}$), as shown in this study, using Eq. (3) and $B_n \approx B_0$ we can make further approximation as follows:

$$\begin{aligned} BL &= B_m L_m + B_n L_n + B_0 L_0 \\ &= (B_s + B_n) L_m + B_n L_n + B_0 L_0 \\ &= B_s L_m + (B_n L_m + B_n L_n + B_0 L_0) \\ &\approx B_s L_m + (B_n L_m + B_n L_n + B_n L_0) = B_s L_m + B_n L, \end{aligned} \quad (11)$$

$$\frac{d\lambda}{dT} \approx \frac{2S}{\lambda} \frac{\delta B_m}{\delta T} L_m = \frac{\lambda}{BL} \frac{\delta B_m}{\delta T} L_m \approx \frac{\lambda}{B_s + B_n L / L_m} \frac{\delta B_m}{\delta T}. \quad (12)$$

Therefore, the temperature sensitivity of the wavelength shift increases with the increase of the temperature sensitivity of the fiber birefringence, and the sensitivity is a function of the wavelength (λ), the fiber birefringences (B_s, B_n), and the ratio between the whole length of the side-hole fiber and that of the indium-filled fiber region (L/L_m). Using the measured birefringent properties of the fiber ($B_s = 9.54 \times 10^{-5}$, $B_n = 1.06 \times 10^{-4}$, and $\delta B_m / \delta T = -3.30 \times 10^{-6} \text{ K}^{-1}$ at 1500 nm) listed in Table 1, Eq. (12) yields $d\lambda/dT = -1500 / (9.54 \times 10^{-5} + 1.06 \times 10^{-4} L/L_m) \times 3.30 \times 10^{-6} \text{ nm/K}$; thus the wavelength-shift sensitivity depends on the length ratio, L/L_m , in the form of $y = -51.89 / (1 + 1.11x)$.

4. Results

Figure 3 shows the measured output spectra of sensor A with indium and the reference sensor without indium. The periodic interference fringes were found in the spectra. In the reference sensor, the fringe spacing was 10.62 nm at 34.4°C near the wavelength of 1500 nm. The spacing decreased to 9.46 nm in sensor A with indium at the similar temperature of 35.2°C; this is due to the birefringence increase induced by indium with the larger thermal expansion coefficient than that of the cladding material, silica glass [11]. In the reference sensor without indium, the interference fringe near 1500 nm slightly shifted (3.9 nm) to the shorter wavelength during the temperature increase from 34.4°C to 42.8°C. The blueshift was attributed to the decrease in the fiber birefringence during the increase of the temperature as explained in previous studies [2,4,11]. In the fiber sensor with indium, the interference fringe shift was very remarkable, and the amount of the blueshift was 51.5 nm during the elevation of the corresponding temperature range from 35.2°C to 42.2°C. In order to obtain the interference-fringe shift spectra of sensor A as shown in Fig. 3(b), we have continuously monitored the variation of the interference fringes during the temperature increase. Then, the spectrum was acquired with the increase of the temperature when the interference fringe shifted every second multiple of the fringe spacing. The arrows marking a particular interference peak represent the guide to trace the wavelength shift.

Figure 4 compares the magnitude of the wavelength shift of the interference fringe near 1500 nm in the fiber-optic sensors during the temperature increase from 25°C to 83°C. In the reference sensor made by the side-hole fiber without indium, the amount of the wavelength shift was ~35 nm during the temperature increase of 60°C. In sensor A with

Table 1. Optical Characteristics of the Fiber-optic Sensor with Indium (Sensor A) and the Reference Sensor

Properties	Fringe Spacing (S)		Birefringence (B _m , B _n)		dS/dT	dB _m /dT, dB _n /dT	dλ/dT
	at 25°C	at 83°C	at 25°C	at 83°C			
Unit	nm	nm	—	—	nm/K	/K	nm/K
With indium	8.98	12.76	2.02 × 10 ⁻⁴	1.55 × 10 ⁻⁵	6.76 × 10 ⁻²	-3.30 × 10 ⁻⁶	-7.38
Without indium	10.62	10.69	1.059 × 10 ⁻⁴	1.046 × 10 ⁻⁴	1.36 × 10 ⁻³	-2.70 × 10 ⁻⁸	-0.70

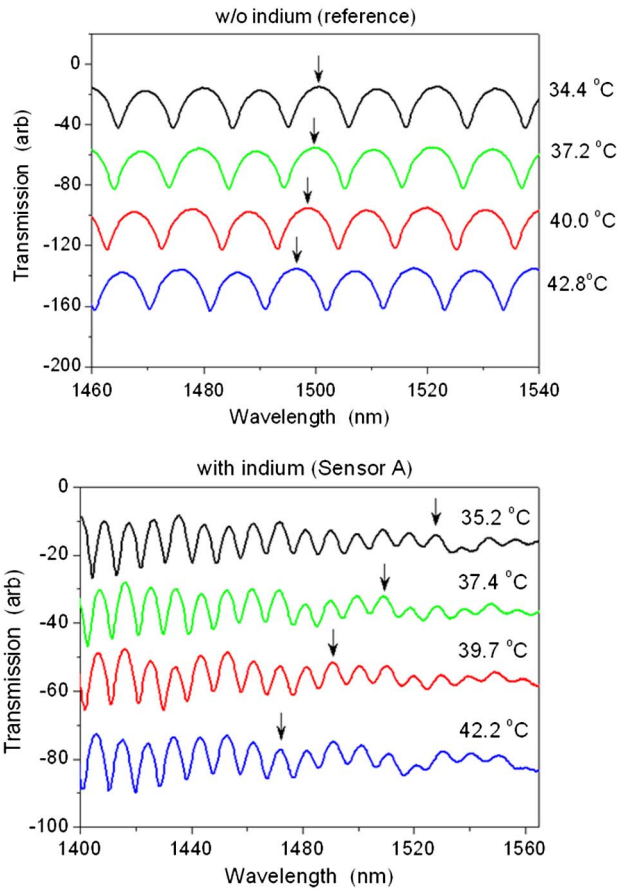


Fig. 3. (Color online) Wavelength shift of the interference fringe in the fiber-optic temperature sensors based on the side-hole fibers without (reference sensor) and with (sensor A) indium. The arrows represent the guide to show the wavelength shifts.

indium, on the other hand, the corresponding wavelength shift was increased more than 12 times, and the shift was 437 nm upon the temperature change. The temperature sensitivity of the wavelength shift, $d\lambda/dT$, of the sensor with indium was -7.38 nm/K, and this was one order larger than the value, -0.70 nm/K, of the reference sensor. To

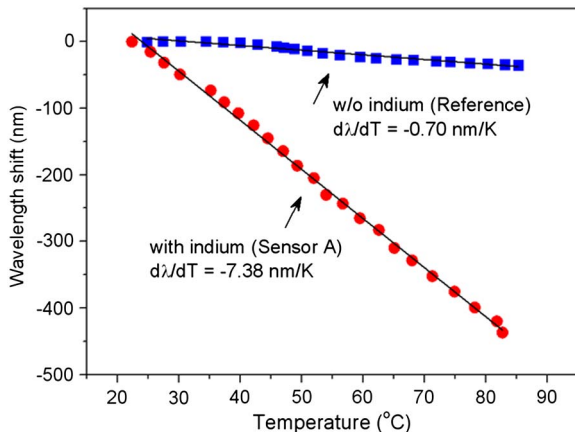


Fig. 4. (Color online) Wavelength shift of the interference fringes near 1500 nm in the fiber-optic temperature sensors with (sensor A) and without (reference sensor) indium in the temperature from 25°C to 83°C.

the knowledge of the authors, the temperature sensitivity of the fiber-optic sensor demonstrated in this study was larger than the values, $d\lambda/dT = -1$ to -2 nm/°C, of the most sensitive sensors reported so far [2,4].

The birefringences of the side-hole fiber with and without indium were investigated to clarify the large temperature sensitivity of the fiber-optic sensor. Figure 5(a) represents the fringe spacings of sensor A and the reference sensor near 1500 nm in the temperature range of $\sim 25^\circ\text{C}$ to 83°C . In the reference sensor, the fringe spacing was 10.62 nm at 24.8°C and slightly increased to 10.69 nm at 83.1°C . As represented in the figure, the fringe spacing with the temperature could be linearly fitted. The temperature sensitivity of the fringe spacing with the increase of the temperature was estimated to be $dS/dT = \sim 1.36 \times 10^{-3}$ nm/K from the slope of the fitted line. In sensor A, the fringe spacings were 8.98 and 12.76 nm at the similar temperatures of 25.4°C and 82.7°C , respectively, and the temperature sensitivity of the fringe spacing ($dS/dT = \sim 6.76 \times 10^{-2}$ nm/K) was much larger than that of the reference sensor. The temperature can be measured from the fringe spacing itself because the fringe

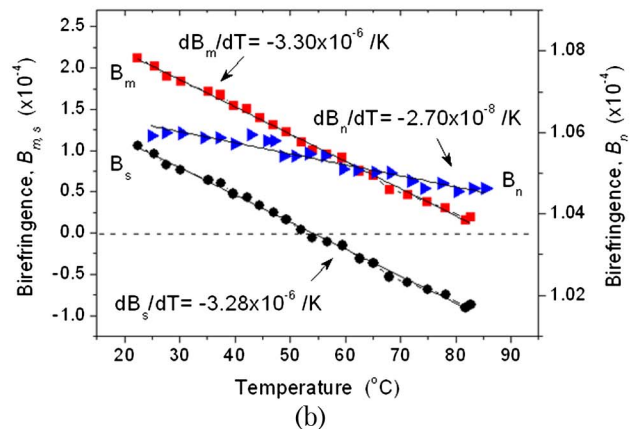
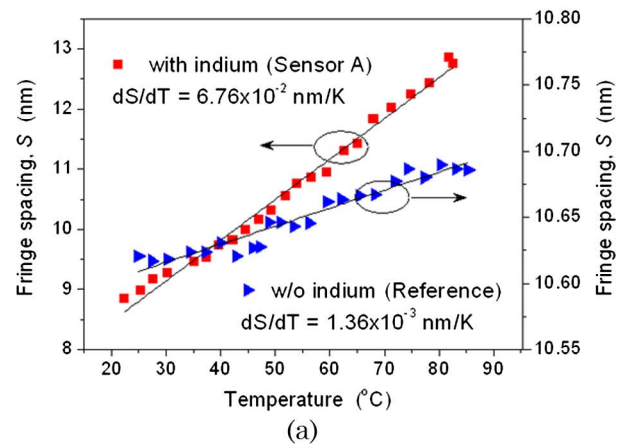


Fig. 5. (Color online) (a) Interference fringe spacing of sensor A with indium and the reference sensor without indium in the temperature range 25°C to 83°C. (b) Birefringence of the fiber regions with and without indium and birefringence solely induced by indium.

spacing as well as the wavelength shift considerably depends on temperature [17]. The temperature sensitivity of the fringe spacing was large enough for temperature sensing. The sensitivity was 18 times larger than the value, 3.70×10^{-3} nm/K, reported in [17]. The temperature resolution of the sensor was estimated to be $\sim 0.15^\circ\text{C}$ from the spectral resolution (0.01 nm) of the optical spectrum analyzer and the temperature sensitivity (6.76×10^{-2} nm/K).

From the measured fringe spacings, the fiber birefringences in the fiber regions with and without indium were calculated using Eqs. (4) and (5), and the results are shown in Fig. 5(b). The birefringence in the fiber region without indium, B_n , was 1.059×10^{-5} at 24.8°C and slightly decreased to 1.046×10^{-5} with the temperature increase up to 83.1°C . The temperature sensitivity of the birefringence was $dB_n/dT = -2.70 \times 10^{-8}/\text{K}$ from the slope of the fitted line. The birefringence in the fiber region with indium, B_m , was 2.02×10^{-4} at 25.4°C and strongly decreased to 1.55×10^{-5} with the temperature increase up to 83.1°C . The temperature sensitivity of the birefringence in the fiber with indium was $dB_m/dT = -3.30 \times 10^{-6}$ and the sensitivity was 122 times enhanced from that of the fiber without indium. The fiber birefringence solely induced by indium, B_s , was also investigated using Eq. (6). The birefringence was 9.54×10^{-5} at 25.4°C and also significantly decreased to -8.67×10^{-5} at 82.7°C ; the temperature sensitivity, dB_s/dT , was $-3.28 \times 10^{-6}/\text{K}$. It is interesting that the sign of B_s changed from positive to negative near 55°C . This unique birefringence property can be explained by the compensation effect between the tensile stress from the thermal expansion of indium (positive effect to the birefringence) and the compressive stress from the applied gas pressure during the indium infiltration process (negative effect to the birefringence) [18]. The positive effect on the birefringence by the thermal property of indium decreased with the increase of temperature while the negative effect on the birefringence by the applied gas pressure did not change regardless of temperature; thus the birefringence became negative at a temperature near 55°C .

In Table 1, optical characteristics of the fiber-optic sensor with indium (sensor A) and the reference sensor are summarized. As a material property, the temperature sensitivity of the birefringence was considerably enhanced by incorporation of indium in the side-hole fiber; thus the dS/dT and $d\lambda/dT$, which depend on the birefringence property of the fiber, also increased. Using Eq. (12) with the fiber lengths (L 100 cm, $L_m = 20$ cm) and the measured birefringent properties (B_m and dB_m/dT) shown in the table, the temperature sensitivity of the wavelength shift was estimated to be $d\lambda/dT = 1500 (-3.30 \times 10^{-6}) / (9.54 \times 10^{-5} + 1.059 \times 10^{-4} \times 100/20) = -7.92$ nm/K, and the estimation showed good agreement with the measured value of $d\lambda/dT = -7.38$ nm/K.

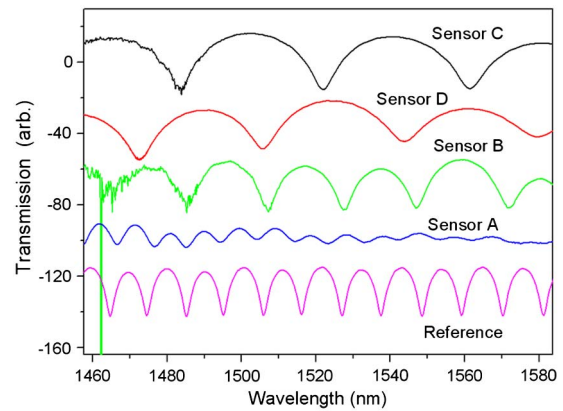


Fig. 6. (Color online) Output spectra of the fiber-optic temperature sensors (sensors A, B, C, and D) made with different lengths of the side-hole fiber and the indium-filled fiber region at $\sim 35^\circ\text{C}$.

Figure 6 shows the measured output spectra of sensors A, B, C, and D made by the different lengths of the side-hole fiber and the indium-filled fiber region at the temperature of $\sim 35^\circ\text{C}$. The interference-fringe spacing of sensor A with L of 100 cm and L_m of 20 cm was 9.46 nm. The fringe spacing of sensor B with the shorter $L = 50$ cm and $L_m = 2$ cm increased to 26.3 nm. In sensor C with the further decreased L of 25 cm and the same L_m of 2 cm, the fringe spacing increased much more to 39.5 nm. In sensor D with L of 25 cm and the longer L_m of 5 cm, the fringe spacing slightly decreased to 35.7 nm from that of sensor C. The length-dependent fringe spacing was well explained by Eq. (3). Because the phase difference increased with the increases of the fiber length and the birefringence, the fringe spacing decreased by the increase of the side-hole fiber length and also by the increase of the length of the indium-filled region even with the side-hole fiber length fixed at a constant. Thus, the fringe spacing of the sensor can be varied by properly changing the lengths of the side-hole fiber and the indium-filled fiber region as well.

Figure 7(a) shows the wavelength shift of the interference fringe in the fiber-optic sensors (sensors B, C, and D) made by the different lengths of the side-hole fiber and the indium-filled fiber region. The wavelength shift was measured near 1500 nm in the temperature range of 28°C – 85°C . As shown in the figure, the negative wavelength shifts increased linearly with the increase of temperature in all types of sensors. In sensor B with $L = 50$ cm and $L_m = 2$ cm ($R = L/L_m = 25$), the temperature sensitivity was -1.83 nm/K. In sensor C with the smaller $R = 12.5$ ($L = 25$ cm, $L_m = 2$ cm), the temperature sensitivity was found to increase to -4.07 nm/K. The temperature sensitivity was much higher, -6.76 nm/K, in sensor D with $R = 5$ ($L = 25$ cm, $L_m = 5$ cm), and the sensitivity became similar to that (-7.38 nm/K) of sensor A with the same R . Figure 7(b) represents the wavelength-shift sensitivity to the fiber-length ratio between the side-hole fiber and the indium-filled region. The sensitivity

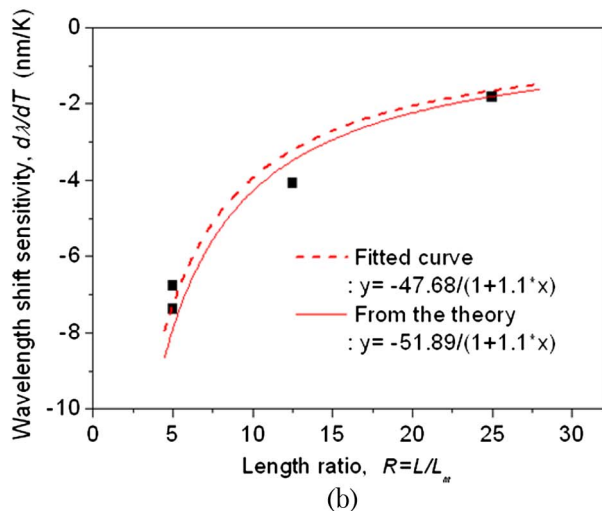
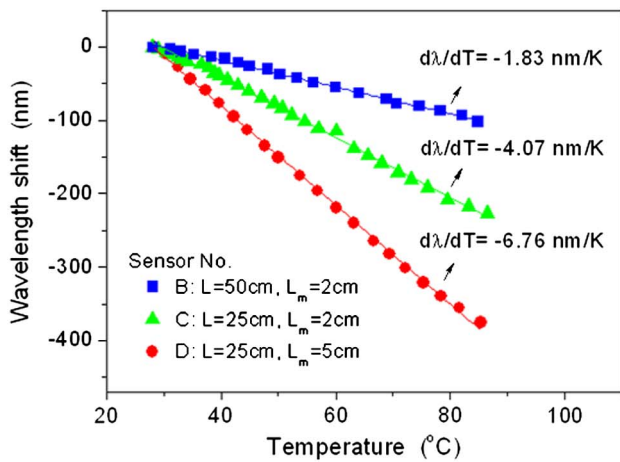


Fig. 7. (Color online) (a) Wavelength shift of the interference fringes in sensors B, C, and D made by different lengths of the side-hole fiber and indium-filled fiber region in the temperature range of 28°C to 85°C. (b) Temperature sensitivity of the wavelength shift with the length ratio between the fiber regions with and without indium. The solid curve was obtained from the theoretical Eq. (12) and the birefringent properties of the fiber ($B_s = 9.54 \times 10^{-5}$, $B_n = 1.06 \times 10^{-4}$, and $\delta B_m/\delta T = -3.30 \times 10^{-6} \text{ K}^{-1}$), and the dashed curve represents the fitting by $y = a/(1+1.11x)$ based on the equation.

was fitted by $y = a/(1+1.11x)$ from the theoretical expectation with Eq. (12). The fitting result of $a = -47.68$ was similar to the value, -51.89 , obtained by using the measured birefringent properties of the fiber (B_s , B_n , and $\delta B_m/\delta T$) as already described in Section 3.

The optical properties and the dimensions of the side-hole fibers used in the sensors are summarized in Table 2. Based on the experimental demonstrations as shown in Figs. 6 and 7, we can deduce that the magnitudes of the fringe spacing and the temperature sensitivity can be controlled by changing the lengths of the side-hole fiber and the indium-filled fiber region. Therefore, the advantageous characteristics of the fiber-optic sensor, such as the high temperature sensitivity, the linearity in the

Table 2. Dimensional and Optical Properties of the Fiber-optic Temperature Sensors*

Sensor No.	L cm	L_p cm	L_m cm	R	S nm	$d\lambda/dT$ nm/K
A	100	50	20	5	9.46	-7.38
B	50	50	2	25	26.3	-1.83
C	25	25	2	12.5	39.5	-4.07
D	25	25	5	5	35.7	-6.76

* R designates the ratio between L and L_m , L/L_m . The interference fringe spacing (S) was measured at $\sim 35^\circ\text{C}$, and the wavelength shift sensitivity ($d\lambda/dT$) was obtained near 1500 nm.

wavelength shift, and the controllabilities in the fringe spacing and the sensitivity make the sensor a potential device for temperature-sensing applications.

5. Conclusion

A fiber-optic temperature sensor based on a side-hole glass optical fiber filled with indium metal has been made, and the optical characteristics of the sensor were experimentally investigated. The fiber-optic sensor exhibited the very high temperature sensitivity of $d\lambda/dT = -7.38 \text{ nm/K}$, and the sensitivity was varied by changing the relative length between the side-hole fiber and the indium-filled fiber region. The dependence of the temperature sensitivity on the relative fiber length was in agreement with the theoretical expectation. It was also found that the temperature sensitivities of the fringe spacing and the fiber birefringence significantly increased more than 49 and 120 times by the incorporation of indium, respectively. The enhancement of the temperature sensitivities resulted from the large thermal expansion property of the indium inside the fiber.

This research work was supported by the National Research Foundation through the research programs (nos. 20100020794 and 2008-0061843), by the Top Brand project (Photonics 2020), by the Asian Laser Center program through grants provided by GIST in 2011, and by the Brain Korea-21 project, Ministry of Education, Science and Technology, South Korea.

References

- V. Bhatia and A. M. Vengsarkar, "Optical fiber long-period grating sensors," *Opt. Lett.* **21**, 692-694 (1996).
- A. N. Starodumov, L. A. Zenteno, D. Monzon, and E. De La Rosa, "Fiber Sagnac interferometer temperature sensor," *Appl. Phys. Lett.* **70**, 19-21 (1997).
- A. D. Kersey, M. A. Davis, H. J. Patrick, M. LeBlanc, K. P. Koo, C. G. Askins, M. A. Putnam, and E. J. Friebele, "Fiber grating sensors," *J. Lightwave Technol.* **15**, 1442-1463 (1997).
- O. Frazao, J. M. Baptista, and J. L. Santos, "Recent advances in high-birefringence fiber loop mirror sensors," *Sensors* **7**, 2970-2983 (2007).
- K. Lee, P. Hu, J. L. Blows, D. Thorncraft, and J. Baxter, "A 200 m optical fiber with integrated electrode and its poling," *Opt. Lett.* **29**, 2124-2126 (2004).
- N. Myren and W. Margulis, "Time evolution of frozen-in field during poling of fiber with alloy electrodes," *Opt. Express* **13**, 3438-3444 (2005).
- B. H. Kim, S. Moon, U. C. Paek, and W.-T. Han, "All fiber polarimetric modulation using an electro-optic fiber with

- internal Pb-Sn electrodes,” *Opt. Express* **14**, 11234–11241 (2006).
8. G. Chesini, C. M. B. Cordeiro, C. J. S. de Matos, M. Fokine, I. C. S. Carvalho, and J. C. Knight, “All-fiber devices based on photonic crystal fibers with integrated electrodes,” *Opt. Express* **17**, 1660–1665 (2009).
 9. J. Hou, D. Bird, A. George, S. Maier, B. Kuhlmeier, and J. C. Knight, “Metallic mode confinement in microstructured fibres,” *Opt. Express* **16**, 5983–5990 (2008).
 10. M. Hautakorpi, M. Mattinen, and H. Ludvigsen, “Surface-plasmon-resonance sensor based on three-hole microstructured optical fiber,” *Opt. Express* **16**, 8427–8432 (2008).
 11. B. H. Kim, S. H. Lee, A. Lin, C.-L. Lee, J. Lee, and W.-T. Han, “Large temperature sensitivity of Sagnac loop interferometer based on the birefringent holey fiber filled with metal indium,” *Opt. Express* **17**, 1789–1794 (2009).
 12. S. H. Lee, B. H. Kim, and W.-T. Han, “Effect of filler metals on the temperature sensitivity of side-hole fiber,” *Opt. Express* **17**, 9712–9717 (2009).
 13. B. H. Kim, S. H. Lee, D. H. Son, T.-J. Ahn, S. Kim, and W.-T. Han, “Highly sensitive temperature sensor based on the side-hole optical fiber filled with indium,” in *Technical Digest of European Conference on Optical Communications* (IEEE, 2011), paper We.10.P1.03.
 14. M. Fokine, L. E. Nilsson, A. Claesson, D. Berlemont, L. Kjellberg, L. Krummenacher, and W. Margulis, “Integrated fiber Mach–Zehnder interferometer for electro-optic switching,” *Opt. Lett.* **27**, 1643–1645 (2002).
 15. D. R. Lide, *Handbook of Chemistry and Physics* (CRC, 2000), Sec. 8.
 16. X. Fang and R. O. Claus, “Polarization-independent all-fiber wavelength-division multiplexer based on a Sagnac interferometer,” *Opt. Lett.* **20**, 2146–2148 (1995).
 17. E. De la Rosa, L. A. Zenteno, A. N. Starodumov, and D. Monzon, “All-fiber absolute temperature sensor using an unbalanced high-birefringence Sagnac loop,” *Opt. Lett.* **22**, 481–483 (1997).
 18. S. H. Lee, D. H. Son, B. H. Kim, and W.-T. Han, “Effect of infiltration pressure on the birefringent properties of a side-hole fiber filled with indium,” *Opt. Lett.* **37**, 2322–2324 (2012).